



Publication Year	2007
Acceptance in OA @INAF	2024-02-02T12:40:47Z
Title	Combination of long time-series of troposphere zenith delays observed by VLBI
Authors	Heinkelmann, R.; Boehm, J.; Schuh, H.; Bolotin, S.; Engelhardt, G.; et al.
DOI	10.1007/s00190-007-0147-z
Handle	http://hdl.handle.net/20.500.12386/34692
Journal	JOURNAL OF GEODESY
Number	81

Combination of long time-series of troposphere zenith delays observed by VLBI

R. Heinkelmann · J. Boehm · H. Schuh ·
S. Bolotin · G. Engelhardt · D. S. MacMillan ·
M. Negusini · E. Skurikhina · V. Tesmer · O. Titov

Received: 5 May 2006 / Accepted: 10 February 2007 / Published online: 10 March 2007
© Springer-Verlag 2007

Abstract Within the International Very Long Baseline Interferometry (VLBI) Service for Geodesy and Astrometry (IVS), long time-series of zenith wet and total troposphere delays have been combined at the level of parameter estimates. The data sets were submitted by eight IVS Analysis Centers (ACs) and cover January 1984 to December 2004. In this paper, the combination method is presented and the time-series submitted by the eight IVS ACs are compared with each other. The combined zenith delays are compared with time-series provided by the International Global Navigation Satellite System (GNSS) Service (IGS), and with zenith delays derived from the European Centre for Medium-Range Weather Forecasts (ECMWF). Before the combination, outliers are eliminated from the individual time-series using the robust BIBER (bounded

influence by standardized residuals) estimator. For each station and AC, relative weight factors are obtained by variance component estimation. The mean bias of the IVS ACs' time-series with respect to the IVS combined time-series is 0.89 mm and the mean root mean square is 7.67 mm. Small differences between stations and ACs can be found, which are due to the inhomogeneous analysis options, different parameterizations, and different treatment of missing in-situ pressure records. Compared to the IGS zenith total delays, the combined IVS series show small positive mean biases and different long-term trends. Zenith wet delays from the ECMWF are used to validate the IVS combined series. Inconsistencies, e.g., long-term inhomogeneity of the in-situ pressure data used for the determination of VLBI zenith delays, are identified.

R. Heinkelmann (✉) · J. Boehm · H. Schuh
Institute of Geodesy and Geophysics,
Vienna University of Technology,
Gusshausstr. 27–29, 1040 Vienna, Austria
e-mail: rob@mars.hg.tuwien.ac.at

S. Bolotin
Main Astronomical Observatory,
National Academy of Sciences of Ukraine,
Akademika Zabolotnoho Str. 27,
03680 Kiev, Ukraine
e-mail: bolotin@mao.kiev.ua

G. Engelhardt
Bundesamt für Kartographie und Geodäsie (BKG),
Karl-Rothe-Str. 10–14, 04105 Leipzig, Germany
e-mail: gerald.engelhardt@bkg.bund.de

D. S. MacMillan
NVI Incorporated and NASA Goddard Space Flight Center
(GSFC), Greenbelt, MD 20771, USA
e-mail: dsm@leo.gsfc.nasa.gov

M. Negusini
Istituto di Radioastronomia (IRA),
Istituto Nazionale di Astrofisica (INAF),
Via P. Gobetti 101, 40129 Bologna, Italy
e-mail: negusini@ira.inaf.it

E. Skurikhina
Institute of Applied Astronomy (IAA),
nab. Kutuzova, 10, St. Petersburg 191187, Russia
e-mail: sea@ipa.nw.ru

V. Tesmer
Deutsches Geodätisches Forschungsinstitut (DGFI),
Alfons-Goppel-Str. 11, 80539 München, Germany
e-mail: tesmer@dgfi.badw.de

O. Titov
Geoscience Australia, PO Box 378, Canberra 2601, Australia
e-mail: Oleg.Titov@ga.gov.au

Keywords Troposphere delays · Intra-technique combination · VLBI

1 Introduction

The troposphere delay is one of the major error sources in the analysis of space-geodetic technique data measured at radio wavelengths. The impact of this error on Very Long Baseline Interferometry (VLBI) parameters was studied in detail by Davis et al. (1985). At that time (1985), only a small number of VLBI observations were available, and the work dealt primarily with theoretical issues. The concept of the troposphere delay was discussed in detail and basic formulas were presented.

Comparisons of zenith wet delays (ZWD) obtained by different techniques have been reported by various authors. For example, Gradinarsky et al. (2000) found that the ZWD obtained by the VLBI and GPS space-geodetic techniques and water vapor radiometer (WVR) agree better in the case of small variability in the troposphere. Their study was limited to 54 days and to one co-located site: Onsala (Sweden). Behrend et al. (2000) analyzed about 2 weeks of data during December 1996 at Madrid (Spain) and reported differences between VLBI and GPS to be smaller than 1 cm. In addition, they suggested extending this type of study to longer time-series. Niell et al. (2001) investigated the results of a 2-week VLBI campaign in August 1995 (CONT95) at Westford (USA), comparing four different techniques: VLBI, GPS, WVR and measurements of radiosondes. In their study, the VLBI technique was found to be the most accurate for the determination of zenith delays.

Data from the continuously observing two-week campaign in October 2002 (CONT02) were analyzed by Snajdrova et al. (2005). In this work, the Doppler Orbitography Radiopositioning Integrated by Satellite (DORIS) system was included in the comparisons and the agreement with the other space-geodetic techniques (VLBI, GPS) in terms of troposphere delays was found to be at a lower level. Since then comparative studies on troposphere parameters have been extended and performed on longer time-series. The International Earth rotation and reference systems service (IERS) launched a combination pilot project (CPP) and announced further parameters, including the troposphere parameters, to be integrated in its future combined products.

Within the International VLBI Service for Geodesy and Astrometry (IVS, Schlueter et al. 2002) troposphere parameters have been already compared and combined in the IVS pilot project troposphere (Schuh and Boehm

2003). However, the combination was limited to the regular IVS-R1 and -R4 weekly 24-h sessions starting in January 2002. Other types of parameters have also been combined: the terrestrial reference frames (TRFs) of various Analysis Centers (ACs) have been transformed into a common VLBI TRF: VTRF2005 (Nothnagel 2005), and Earth orientation parameters (EOPs) are routinely combined at the normal equation level at the Geodetic Institute of the University of Bonn (Germany).

In contrast to the combination at the level of normal equations, the troposphere parameters are combined at the level of parameter estimates. Among the other technique centers of the IERS, the International Global Navigation Satellite System (GNSS) Service (IGS) has established a troposphere combination working group, where the results of eight IGS ACs are combined on a weekly basis (Gendt 2004). Troposphere parameters of IVS and IGS were combined using the CONT02 campaign data at the ITRS Combination Center of the Deutsches Geodätisches Forschungsinstitut (DGFI), Munich (Germany) (Krügel et al. 2007).

The eight IVS ACs listed in Table 1 provided long time-series (most of them from January 1984 until December 2004) of troposphere zenith delay (ZD), i.e., zenith wet delay (ZWD) and zenith total delay (ZTD), to the Institute of Geodesy and Geophysics, Vienna (Austria), for comparison and combination. The long time-series of ZDs are determined using all geodetic VLBI sessions since January 1984 that are available from IVS Data Centers. Currently, combined time-series are available for 50 VLBI stations that either observe in current networks or have observed in at least 20 sessions covering at least 2 years in VLBI's observational history. The only mobile antenna included is the TIGO (transportable integrated observing system) at Wettzell (Germany) and at Concepción (Chile), where it is currently mounted.

The combined IVS zenith delay series are available from IVS Data Centers, e.g., from the ftp-server of the Bundesamt für Kartographie und Geodäsie (BKG), Germany. We investigate troposphere zenith delay time-series and focus on the 12 most frequently used IVS network stations (Behrend and Baver 2005) listed in Table 3 (later). Each of the 12 VLBI stations is co-located with a GPS site. In the first section, the troposphere parameters are introduced and the software, geophysical models, and analysis options used by the individual IVS ACs are presented. Then, the outlier elimination process and weighting scheme of the combination are discussed. Thereafter, the individual solutions of the IVS ACs are compared with the combined solution to obtain a realistic measure of precision.

Table 1 The eight IVS Analysis Centers contributing to the combination of long time-series of troposphere parameters

AC	Full name, city, country
AUS	Geoscience Australia, Canberra, Australia
BKG	Bundesamt für Kartographie und Geodäsie, Leipzig, Germany
CNR	Istituto di Radioastronomia - CNR, Bologna, Italy
DGF	Deutsches Geodätisches Forschungsinstitut, Munich, Germany
GSF	NVI Inc. and NASA Goddard Space Flight Center, Greenbelt, USA
IAA	Institute of Applied Astronomy, Russian Academy of Sciences, St. Petersburg, Russia
IGG	Institute of Geodesy and Geophysics, Vienna University of Technology, Vienna, Austria
MAO	Main Astronomical Observatory, National Academy of Sciences of Ukraine, Kiev, Ukraine

The comparison of the IVS combined series with series from the IGS and the European Centre for Medium-Range Weather Forecasts (ECMWF) allows a thorough validation of the IVS combined ZD series, as shown in the last part of this paper. The comparison of long time-series of troposphere zenith delays provides an insight to the intra-technique and inter-technique consistency of troposphere parameters and correlated parameters, in particular the station’s height component. However, the ultimate goal is to obtain information for meteorology and climatology, such as the precipitable water vapour (Bevis et al. 1994), which can be derived from ZWDs.

2 Troposphere models, data, and software packages

2.1 Troposphere parameters

Measurements by space-geodetic techniques at radio wavelengths, VLBI, GNSS or DORIS, are systematically delayed by the dry and wet constituents of the troposphere. The corresponding data analysis of observations with these techniques allows one to estimate troposphere ZDs with mm-accuracy. Multiplication of the ZDs with the corresponding wet and hydrostatic mapping functions yields the line-of-sight (LoS) delays.

The troposphere parameters estimated in most of the conventional VLBI analyses are the atmosphere gradient components in the north and east directions, G_N and G_E , respectively, and the zenith non-hydrostatic delay that accounts for the integrated delay caused mainly by the wet constituents of the troposphere and therefore often called ZWD. The signal delay L (mm) caused by the troposphere (strictly speaking the non-dispersive ‘neutral’ atmosphere) depends on the elevation e and the azimuth a of an observation. An often-used parameterization is:

$$L(e, a) = m_h(e) \cdot ZHD + m_w(e) \cdot ZWD + m_g(e) \cdot \cot(e) [G_N \cdot \cos(a) + G_E \cdot \sin(a)] \tag{1}$$

where ZHD (mm) denotes the zenith hydrostatic (dry) delay and ZWD (mm) denotes the zenith wet delay. The hydrostatic and wet mapping functions $m_{h,w}$ (unitless) are assumed to be known, and the gradient mapping functions m_g can be either the wet or the hydrostatic troposphere mapping functions (MacMillan 1995).

Currently, three different mapping functions are applied by the IVS ACs, contributing to this combination: the Vienna Mapping Functions (VMF) (Boehm and Schuh 2004), the New Mapping Functions (NMF) (Niell 1996), and the MIT Temperature Mapping Functions (MTT) (Herring 1992). The NMFs are also called Niell Mapping Functions by some authors.

The zenith total delay (ZTD) (mm) is the sum of the zenith hydrostatic and wet delays:

$$ZTD = ZHD + ZWD \tag{2}$$

In the analysis, ZTD is determined as the sum of the zenith a priori delay and the estimated zenith residual delay. In GPS analysis, the ZTD is sometimes called zenith path delay (ZPD), or zenith delay estimates. However, the latter is misleading, because sometimes an a priori delay is considered and the zenith delay estimates equal the corrections to the a priori delays.

As the a priori delays are usually mapped with the hydrostatic mapping function and the estimated delays with the wet mapping function, systematic errors are introduced when the a priori delays significantly deviate from the hydrostatic delays. This is the case when a standard troposphere model is used (e.g. Berg 1948). To avoid such mapping errors, the a priori delays have to equal the hydrostatic delays, which are usually obtained by a formula of Saastamoinen (1973) modified by Davis et al. (1985) (in metres):

Table 2 Analysis options, software packages, models and parameterizations applied by the IVS ACs contributing to the combination of long time-series of troposphere parameters

AC	Software package	Zenith delay model	Mapping functions	Elevation cutoff angle ^o	TRF a priori	TRF estimated	CRF estimated	Dwnwght. of low elev. obs.
AUS	OCCAM	LSCM	VMF	5	ITRF2000	Global	Global	Yes
BKG	CALC/SOLVE	PWLF	NMF	5	VTRF2003	Global	Global	No
CNR	CALC/SOLVE	PWLF	NMF	5	ITRF2000	Local	Fixed	No
DGF	OCCAM	PWLF	VMF	5	ITRF2000	Fixed	Fixed	No
GSF	CALC/SOLVE	PWLF	NMF	3	ITRF2000	Global	Global	No
IAA	OCCAM	RW	VMF	0	VTRF2003	Fixed	Fixed	Yes
IGG	OCCAM	PWLF	VMF	5	VTRF2003	Local	Fixed	No
MAO	SteelBreeze	RW	MTT	0	ITRF2000	Local	Fixed	No

Explanations and references of the individual models are given in the text

LSCM least-squares collocation method, *PWLF* piecewise linear function, *RW* random walk stochastic process, *VMF* Vienna mapping functions, *NMF* new mapping functions (also called ‘Niell mapping functions’), *MTT* MIT temperature mapping functions, *TRF* terrestrial reference frame, *CRF* celestial reference frame

$$\text{ZHD} = \frac{0.0022768 \cdot p_0}{1 - 0.00266 \cdot \cos(2\phi) - 0.00028 \cdot H} \quad (3)$$

The latitude ϕ and the height above the geoid H (km) of the site do not have to be known very accurately (metre-level) for the use of Eq. (3) (Nothnagel 2000). For the total pressure p_0 (hPa), automatically recorded in-situ pressure measurements are usually used.

Unlike the two other input parameters to Eq. (3), the total pressure p_0 has to be known more accurately (to about 0.3 hPa) and homogeneously in order to separate zenith hydrostatic and wet delays. For instance, a shift in the total pressure data by 1.0 hPa corresponds to a shift in the zenith hydrostatic delays by 2.3 mm used as a priori and about the same shift with the opposite sign in the estimated ZWD.

In-situ pressure records often suffer from outliers and missing values, and have to be edited in an appropriate way before the analysis. In order to provide long-term consistency, the in-situ pressure records have to be homogenized, i.e., significant shifts of the running mean value have to be removed (see Heinkelmann et al. 2005a). If the in-situ pressure records are not corrected for the height difference between the pressure sensors and the antenna reference points, station-dependent systematic biases are introduced into the hydrostatic delays and propagate to the ZWDs.

2.2 Software, models, and analysis options

The solutions of the IVS ACs contributing to this combination are computed by three independent software packages (Table 2): OCCAM, CALC/SOLVE, and SteelBreeze. CALC/SOLVE is maintained by the NASA Goddard Space Flight Center (GSFC), SteelBreeze by the Main Astronomical Observatory, National Academy

of Sciences of Ukraine (MAO). The versions of OCCAM at the Institute of Applied Astronomy (IAA), Russia, on the one hand, and at Geoscience Australia, DGF and Institute of Geodesy and Geophysics (IGG), Vienna University of Technology, Vienna, Austria (Titov et al. 2004), on the other hand, have been developed independently from each other.

The current VLBI software packages use different models for the ZWD (Table 2):

- a continuous linear spline function defined at equidistant time intervals, a piecewise linear function (PWLF),
- a random walk stochastic process (RW),
- a least-squares collocation method (LSCM), where the ZWD is assumed to follow a stationary stochastic process specified by a covariance function and finite standard deviation (Titov and Schuh 2000).

For PWLF modelling, the troposphere estimates are at full integer hours covering the approximately 24 h of a usual VLBI session. The RW series are determined by different numerical algorithms: IAA uses a Kalman filter and MAO applies a square root information filter (Bierman 1977).

It has been shown that long time-series of ZDs differ systematically when applying different analysis options. The analysis method and the threshold of outlier detection, the elevation cutoff angle, and the down-weighting of low-elevation observations determine the number and weights of observables used in the analysis, which ultimately affects the ZD estimates and their formal errors (Heinkelmann et al. 2005b). In addition to the analysis options given in Table 2, systematic differences can be due to different parameterizations (e.g.

troposphere gradients of different temporal length) and selection of the a priori coordinates and velocities of the terrestrial reference frames (TRFs) and the celestial reference frames (CRFs), or the geodetic datum definitions.

Troposphere parameters submitted by AUS, BKG, and GSF (cf. Table 2) were estimated in a global solution, i.e., together with station coordinates and velocities, and source coordinates, whereas the other ACs fixed the a priori station coordinates and velocities, or estimated the coordinates per session (locally). The ACs contributing to this combination applied a priori station coordinates and velocities from the ITRF2000 (Altamimi et al. 2002) or the VTRF2003 (Nothnagel 2003). A priori source coordinates were taken from the IERS Celestial Reference Frame [ICRF (Ma et al. 1998)], its first extension, ICRF-Ext.1 (Gambis 1999) or its second extension, ICRF-Ext.2 (Fey et al. 2004). As a requirement for the combination, the zenith delays (ZTD, ZWD) had to be provided at integer hours with a time-resolution of 1 h, i.e., at 18:00 UT, 19:00 UT, etc. The solution settings were left to the analysts, enabling maximum flexibility to achieve the best-possible individual results.

3 Combination of long time-series of zenith delays from IVS ACs

For each integer hour for which at least two ACs report ZDs, a combined ZD is computed in a stepwise procedure. Outliers are eliminated from each time-series using the BIBER (bounded influence by standardized residuals) estimator. Then, relative weight factors are determined by variance component estimation (VCE) for each station and AC. These are used to compute the combined ZDs as a weighted sum of the individual AC ZDs. This procedure is done for the ZWDs and for the ZTDs of each of the stations separately.

3.1 Mathematical model of long time-series of troposphere zenith delays

3.1.1 Stochastic model

Since the individual solutions of the ACs are determined from the same VLBI observations, correlations between the solutions of the ACs appear and should be accounted for (Steinforth and Nothnagel 2004). However, in VLBI analysis, a large variety of models, parameterizations and analysis options are applied (Sect. 2.2); hence, we assume that the solutions of the ACs can be considered

to be independent, i.e., the correlations between solutions are assumed to be zero.

In the uncorrelated case, the stochastic model reduces from a full (N, N) variance-covariance matrix to the reported $(N, 1)$ vector of variances, where N denotes the total number of ZDs for the entire time-span at a station reported by one AC, or reported by all ACs in the case of the combined model.

The reported standard deviations of ZD, determined by various least-squares methods (Gauss-Markov model, Kalman filter, square root information filter, least-squares collocation) and interpolations, show a completely inhomogeneous structure. Using these standard deviations leads to unrealistic weighting of individual observations among the ACs, which cannot be overcome by the estimation of relative weight factors. Therefore, the standard deviations are neglected during the combinations, which simplifies the stochastic model to an $[N, N]$ identity matrix I_N , or an $[N, 1]$ unit vector, respectively. The weight matrices P are set to identity matrices before the outlier detection in order to prevent this process from distortions.

3.1.2 Functional model

The expectation value of the ZWDs and ZTDs can be described by a time-series model considering trend and seasonal components (e.g. Koch 1997, p. 240). For the trend component, a polynomial expansion, i.e., an offset and a linear trend, and for the seasonal component, sinusoids of annual and semi-annual periods are included in the mathematical model (Schuh et al. 2006). The coefficients of the mathematical model are estimated by the BIBER-estimator (Sect. 3.2.1) with an additional normal-distributed error component.

Figure 1 presents spectra of ZWD for Ny-Ålesund (Spitsbergen, Norway) and Gilcreek (Fairbanks, Alaska, USA), including the discrete Fourier transformation (DFT), the Lomb-Scargle periodogram (Lomb 1976), and the cleaned spectrum (Roberts et al. 1987) derived by the CLEAN algorithm (with a g-factor of 0.1 and the maximal number of iterations set to 600). Peaks at annual and semi-annual periods can be identified from the three spectra. Against our expectations, the semi-annual signals are quite pronounced at stations with high latitudes, such as Ny-Ålesund (latitude: 79°) and Gilcreek (latitude: 65°).

Due to the non-equidistant sampling of the ZWD, the spectrum obtained by DFT shows artificial variations at higher periods (>1 year), which do not appear in the Lomb-Scargle periodogram or in the cleaned spectrum. As a consequence, we restrict the functional model to those periods, which can be found in all three spectra.

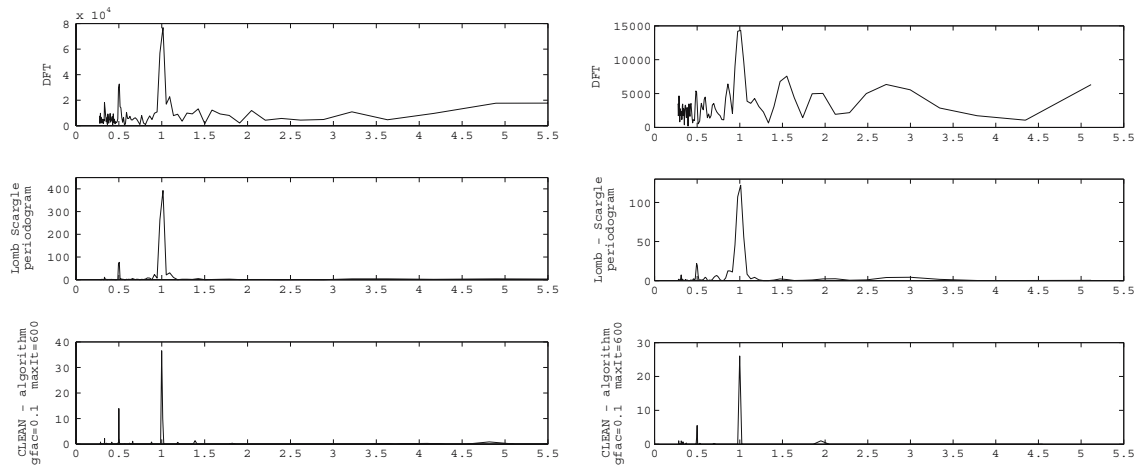


Fig. 1 Fourier spectra of ZWD obtained by IGG for station Gilcreek, Alaska (*left*) and station Ny-Ålesund, Spitsbergen (*right*). Discrete Fourier transform, DFT (*top*), Lomb-Scargle periodogram (*middle*), and CLEAN - algorithm (*bottom*). Units of the periods are years. The DFT and CLEAN-algorithm yield the real semi-amplitude of the power. The Lomb-Scargle periodogram gives the normalized power. The variations at longer periods

(> 1 year) inherent in the spectra obtained by DFT cannot be seen in the Lomb-Scargle periodogram or in the CLEAN spectra and probably arise from the unequally spaced data. Peaks at annual and semi-annual periods can be found in the three spectra at the two stations and at the other stations (not shown here). See text for references and discussion

Equation (4) gives the mathematical model of the long time-series of ZWD and ZTD:

$$Y(t) = a + b \cdot t + A_1 \cdot \sin(2\pi f_1 t) + B_1 \cdot \cos(2\pi f_1 t) + A_2 \cdot \sin(2\pi f_2 t) + B_2 \cdot \cos(2\pi f_2 t) + U(t) \quad (4)$$

where a and b denote coefficients of the offset, and linear trend component; $A_{1,2}$ and $B_{1,2}$ are coefficients of the seasonal component with frequencies $f_{1,2} = \frac{1}{T_{1,2}}$ corresponding to annual T_1 and semi-annual periods T_2 . $U(t)$ denotes a normal-distributed error process with an expectation value of zero and time-independent variance. The seasonal component amplitudes $C_{1,2}$ are determined by:

$$C_{1,2} = \sqrt{A_{1,2}^2 + B_{1,2}^2} \quad (5)$$

3.2 Outlier elimination by the BIBER-estimator

3.2.1 General description of the BIBER-estimator

Outliers are found by the BIBER (bounded influence by standardized residuals) estimator (Wicki 2001). This robust estimator reliably detects outliers, i.e., it avoids errors of the first kind (an outlier is not identified) and of the second kind (an observation is erroneously identified as an outlier), and has small computational costs (Kutterer et al. 2003).

The initial values of this iterative algorithm are obtained by a standard least-squares estimation based on the linearized Gauss-Markov model:

$$Ax = l + v, \quad K_{ll} = \sigma_0^2 Q_{ll} = \sigma_0^2 P_{ll}^{-1} \quad (6)$$

where A denotes the $[N, 6]$ design matrix, x the $[6, 1]$ vector of unknown coefficients or parameters (Eq. 4), l the $[N, 1]$ vector of ZWD or ZTD values from an individual AC for one station over the entire time span, v the $[N, 1]$ vector of residuals, K_{ll} the $[N, N]$ variance-covariance matrix of the ZD, σ_0^2 the theoretical variance factor, and Q_{ll} and P_{ll} the corresponding cofactor matrix and weight matrix.

Initial estimates of the unknown coefficients in the least-squares sense are obtained by:

$$\hat{x} = (A^T P_{ll} A)^{-1} A^T P_{ll} l \quad (7)$$

After a homogenization (e.g. Koch 1997, p. 168), the weight matrix equals the identity matrix. Equation (7) then reads:

$$\hat{x} = (A^T A)^{-1} A^T l \quad (8)$$

The residuals \hat{v} are determined by:

$$\hat{v} = A\hat{x} - l \quad (9)$$

At this point, the parameters \hat{x} and residuals \hat{v} are the results of an ordinary least-squares estimation. Now, the BIBER estimator continues with the cofactor matrix of

the residuals $Q_{\hat{v}\hat{v}}$, the standard deviation of the n th residual $(\sigma_{\hat{v}})_n$ and the standardized residual v_n , expressed as:

$$Q_{\hat{v}\hat{v}} = I_N - A \left(A^T A \right)^{-1} A^T \tag{10}$$

$$(\sigma_{\hat{v}})_n = \sigma_0 \sqrt{(q_{\hat{v}\hat{v}})_{nn}} \tag{11}$$

$$v_n = \frac{\hat{v}_n}{(\sigma_{\hat{v}})_n} \tag{12}$$

where, again, N denotes the number of ZWD or ZTD estimates for an individual AC for the current station, I_N is the $[N, N]$ identity matrix, σ_0 is the square root of the theoretical variance factor σ_0^2 , $(q_{\hat{v}\hat{v}})_{nn}$ is the n th diagonal element of the cofactor matrix of the residuals $Q_{\hat{v}\hat{v}}$, and \hat{v}_n is the n th residual.

Now and at the beginning of each iteration step, the observation with the largest absolute value of the standardized residuals will be considered to be an outlier if the absolute value of its standardized residual exceeds a constant c . Wicki (1992, 1999) suggests a threshold value of c between 2 and 4, which corresponds to two to four times the standard deviation in the case of a normal distribution.

Considering Eq. (7), it becomes obvious that a single outlying observation can change all the estimated coefficients \hat{x} . Consequently, applying Eq. (9), the estimates of the residuals \hat{v} are also affected by the changed vector \hat{x} . This well-known characteristic of the least-squares adjustment is the reason for its non-robustness. The errors of one or more observations propagate directly into the parameters. Robust estimators limit the effect of outlying observations on the parameters.

Unlike the standard robust estimators, e.g., the Huber-estimator (Huber 1981) or the Hampel-estimator (Hampel et al. 1986) the algorithm of the BIBER estimator applies only one modification during one iteration step. This important characteristic allows one to consider the effect of a single observation on the parameters and consequently on the residuals, which are used as the criterion for the identification of outliers.

Generally, different modifications are possible to reduce the effect of an outlier, e.g., the normal equation matrix, the weight of the outlier, or the outlier itself, can be modified in an appropriate way. However, modifying the outlying observation reduces the computational costs, because the normal equation matrix ($A^T P A$) remains unchanged and does not have to be inverted during each iteration step. The version with modification of observations is explained here; see Wicki (2001) for the other procedures.

With the constant cofactors $q_{\hat{v}\hat{v}}$ of Eq. (10), the n th residual $\hat{v}_n^{(m)}$ in the m th iteration step becomes:

$$\hat{v}_n^{(m)} = - \sum_{k=1}^n (q_{\hat{v}\hat{v}})_{nk} \cdot l_k^{(m-1)} \tag{13}$$

The considered outlier is modified in such a way that the absolute value of its residual equals the variable threshold $k_n = c \cdot (\sigma_{\hat{v}})_n$:

$$l_n^{(m)} = l_n^{(m-1)} + \frac{\hat{v}_n^{(m)} - \text{sign}(\hat{v}_n^{(m)}) \cdot k_n}{(q_{\hat{v}\hat{v}})_{nn}} \\ = l_n^{(m-1)} + \frac{d_n^{(m)}}{(q_{\hat{v}\hat{v}})_{nn}} \tag{14}$$

The modification (Eq. 14) is only applied to the observation with the largest absolute value of the standardized residual within one iteration step. It is the smallest possible modification, because thereafter the absolute value of the standardized residual lies exactly at the threshold k_n and the observation just fulfils the distribution assumption within the c -fold standard deviation. The variable threshold k_n accounts for the reliability of the observations at the same time, i.e., if the reliability of the n th observation is small, its partial redundancy $(q_{\hat{v}\hat{v}})_{nn}$, as well as its threshold k_n will also be automatically small. Therefore, the BIBER-estimator is able to detect outliers in leverage points.

The modifications of each iteration step are accumulated in the vector of modifications:

$$\Delta l_n^{(M)} = \frac{1}{(q_{\hat{v}\hat{v}})_{nn}} \sum_{m=1}^M d_n^{(m)} \tag{15}$$

where M denotes the total number of iterations. In contrast to the unmodified residuals \hat{v} in Eq. (9), the modified residuals \hat{v}_{rob} , regarding the robust modifications, are determined by:

$$\hat{v}_{\text{rob}}^{(M)} = A \hat{x}^{(M)} - \left(I + \Delta l^{(M)} \right) \tag{16}$$

where $\hat{x}^{(M)}$ denotes the final robust estimate of the coefficients:

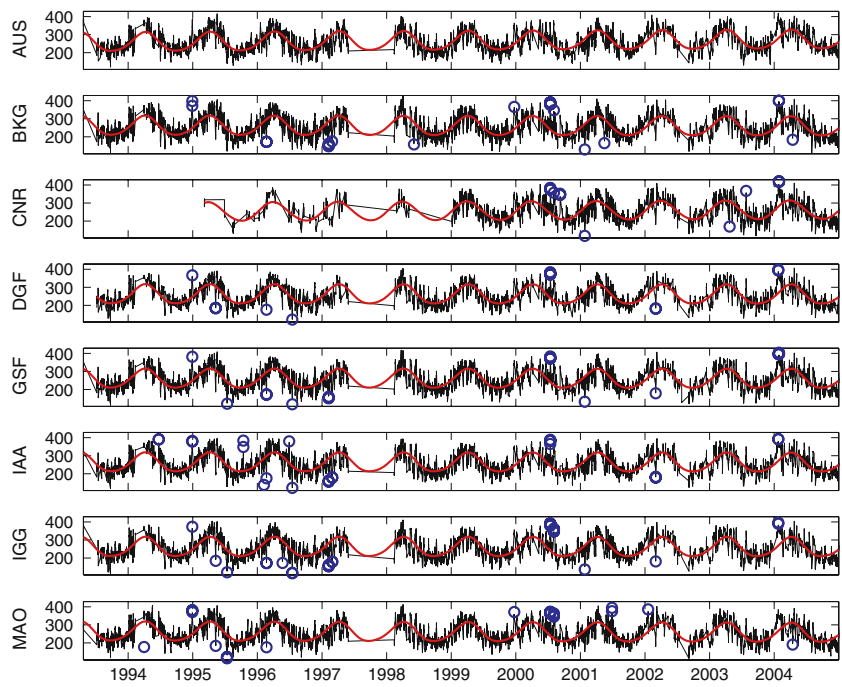
$$\hat{x}^{(M)} = \hat{x} + \left(A^T A \right)^{-1} A^T \Delta l^{(M)} \tag{17}$$

The iterative process is stopped when the absolute values of the standardized residuals satisfy the condition:

$$|v_n| < c \tag{18}$$

The homogenized model has to be retransformed before any additional computations can be performed. If further quantities, e.g., the variance-covariance matrix of the estimated coefficients $K_{\hat{x}\hat{x}}$, are to be determined, the modifications of the observations can be avoided

Fig. 2 Outlier-free time-series of ZWD at Fortaleza, Brazil, from the eight IVS ACs contributing long time-series of troposphere parameters. Eliminated outliers—highlighted with blue circles—were found by the BIBER estimator (Sect. 3.2.1) with respect to the model presented in Eq. (4), which is plotted in red. Units of ZWD are mm and the time is given in years



and instead fictitious weights \tilde{p}_n are used:

$$\tilde{p}_n = \frac{(\hat{v}_{\text{rob}})_n}{(\hat{v})_n} \tag{19}$$

3.2.2 The BIBER-estimator as applied in this study

The treatment of outliers is an essential step of preprocessing, because the subsequent computations rely on the assumption of normally distributed residuals. Therefore, we apply the BIBER estimator with a few changes. Since we neglect the standard deviations reported by the ACs, the homogenization becomes obsolete. After the iterative process of the BIBER estimator stops, inherent outliers are identified. Now, instead of using fictitious weights or modified observations, we neglect the outlying observations, i.e., they are marked as outliers and will not contribute to the combination at all.

Our approach is more rigorous than the original BIBER estimator, but also more consequent, since we will go on neglecting the reported standard deviations all through the combination. Figure 2 presents the outlier-free ZWD time-series at station Fortaleza (Brazil), together with the mathematical model (Eq. 4) obtained from each contributing AC. The empirical threshold value c is set to three, which allows one to identify outliers from all the reported time-series.

3.3 Computation of relative weight factors by variance component estimation

For the determination of variance components, the outlier-free ZWD (or ZTD) estimates are stacked to a combined Gauss-Markov model and extended by one unknown variance factor σ_i^2 for each AC and station. The variance components are determined applying the algorithm of Foerstner (1979), as given by Koch (1997). Then, relative weight factors are obtained:

$$w_i = \frac{\frac{1}{\sigma_i^2}}{\sum_{i=1}^I \frac{1}{\sigma_i^2}} \tag{20}$$

where i indicates the individual AC, and I is the total number of ACs contributing to a station.

3.4 Determination of the combined IVS time-series of zenith wet and total delays

Combined time-series of ZWD and ZTD, respectively, are determined for each station separately on the basis of outlier-free hourly values. At each epoch, where at least two ACs report an hourly value, a combined value is determined by the weighted mean of the hourly values of the ACs applying the relative weight factors (Sect. 3.3) determined by VCE. For the combination, the reported standard deviations are again not regarded.

Table 3 Relative weight factors (Eq. 20) of ZWD obtained by VCE of the 12 most frequently used IVS network stations (Behrend and Baver 2005)

Station	AUS	BKG	CNR	DGF	GSF	IAA	IGG	MAO
ALGOPARK	1.09	0.98	1.04	1.05	1.00	0.96	0.90	0.98
FORTLEZA	0.98	0.98	0.90	1.05	1.02	1.02	1.02	1.03
GILCREEK	0.71	1.04	1.11	1.11	1.07	0.99	1.00	0.98
HARTRAO	0.99	0.96	0.94	1.13	1.02	0.98	0.97	1.02
HOBART26	0.94	0.94	0.97	1.27	1.00	0.90	1.04	0.94
KOKEE	1.04	0.97	0.89	1.03	1.01	1.04	1.00	1.03
MATERA	0.99	0.97	0.96	1.02	1.01	1.06	1.00	1.00
NYALES20	0.93	0.95	0.99	1.17	1.00	0.93	0.99	1.06
SESHAN25	1.02	0.89	1.08	1.11	0.92	1.10	0.92	0.96
TSUKUB32	1.03	0.95	1.00	1.08	0.99	1.00	0.92	1.04
WESTFORD	0.92	0.98	1.21	1.04	0.98	0.98	0.93	0.98
WETTZELL	0.59	1.07	1.18	1.16	1.11	1.06	0.85	0.99
Mean	0.94	0.97	1.02	1.10	1.01	1.00	0.96	1.00

Table 4 Relative weight factors (Eq. 20) of ZTD obtained by VCE of the 12 most frequently used IVS network stations (Behrend and Baver 2005). AUS does not provide zenith total delays

Station	BKG	CNR	DGF	GSF	IAA	IGG	MAO
ALGOPARK	0.95	1.07	1.02	0.97	1.01	0.93	1.05
FORTLEZA	0.98	0.89	1.04	1.01	1.02	1.01	1.05
GILCREEK	1.04	0.96	1.03	1.02	0.96	0.94	1.04
HARTRAO	1.00	0.93	1.09	1.03	0.96	0.98	1.02
HOBART26	0.96	0.95	1.12	1.01	0.97	0.98	1.00
KOKEE	0.97	0.89	1.04	1.00	1.04	1.01	1.05
MATERA	0.96	0.99	1.02	1.01	1.02	0.99	1.00
NYALES20	1.00	0.94	1.03	1.02	0.99	0.97	1.04
SESHAN25	0.91	1.11	1.13	0.93	1.03	0.92	0.99
TSUKUB32	0.97	1.01	1.05	0.99	1.01	0.92	1.05
WESTFORD	0.98	1.14	1.01	0.99	0.96	0.93	0.99
WETTZELL	1.03	1.09	1.09	1.05	1.01	0.76	0.97
Mean	0.98	1.00	1.06	1.00	1.00	0.95	1.02

$$ZD_{\text{comb}} = \sum_{i=1}^I \frac{w_i}{\sum w} \cdot ZD_i \tag{21}$$

where $I \geq 2$. If an AC does not report an estimate, or the reported estimate was marked as an outlier, the AC does not contribute to the combined ZD.

4 Results and discussion

4.1 Relative weight factors

The relative weight factors w_i reflect how well the outlier-free ZDs fit the combined mathematical model. Generally, the relative weight factors are about 1 ± 0.1 , which indicates the overall consistency of the individual solutions. As can be seen in Tables 3 and 4, the relative weight factors of the ACs differ significantly among

the stations, but marginally between ZWD and ZTD. This approves the usage of station-dependent weights instead of a single weight per AC.

Among the eight IVS ACs contributing long time-series of ZDs, the solution of DGFI obtains relative weight factors larger than the average for all the 12 stations analysed in this study, which shows the good quality of this solution. The relative weight factors of the other ACs vary around the average. The relative low weight factors of AUS and IGG for station Wettzell (Germany) are due to larger scatter in the early years of observations until about 1989.0, because atmospheric loading corrections (e.g. Petrov and Boy 2004) and antenna thermal deformation corrections (e.g. Skurikhina 2001) are not applied. In particular, the uncorrected thermal deformations at Wettzell (Germany) antenna introduce seasonal variations in the radial component (Titov and Yakovleva 2000) and degrade the corresponding

Table 5 Bias and RMS of ZWD with respect to the IVS combined solution in mm

Coefficient	AUS	BKG	CNR	DGF	GSF	IAA	IGG	MAO	STD (bias) mean (RMS)
ALGOPARK (Algonquin Park, Canada)									
Bias	-0.79	0.85	0.33	0.23	0.79	0.67	-0.62	-1.41	0.84
RMS	11.91	6.77	5.57	4.73	5.60	8.39	7.43	8.35	7.34
FORTLEZA (Fortaleza, Brazil)									
Bias	3.39	-0.90	-0.83	-0.49	-0.71	0.90	-0.78	-0.70	1.49
RMS	13.35	6.60	8.31	5.10	4.98	7.69	5.69	7.73	7.43
GILCREEK (Fairbanks, Alaska)									
Bias	0.90	-0.27	-0.75	-0.95	-0.34	1.90	-0.11	-0.45	0.95
RMS	13.97	4.91	3.28	4.12	4.77	6.63	6.36	7.25	6.41
HARTRAO (Hatebeesthoek, South Africa)									
Bias	0.32	0.93	0.15	0.36	0.03	-1.21	-0.13	-0.69	0.48
RMS	13.94	9.07	8.23	5.91	6.42	11.58	10.05	10.06	9.41
HOBART26 (Hobart, Tasmania)									
Bias	0.68	0.90	0.71	0.53	-0.86	0.88	-1.63	-0.21	0.94
RMS	15.94	9.79	7.72	6.64	7.34	14.27	8.09	10.41	10.0
KOKEE (Kokee Park, Kauai, Hawaii)									
Bias	1.80	-0.06	-0.02	-0.61	0.11	0.51	-1.12	-0.72	0.90
RMS	8.28	5.82	6.06	4.32	4.82	6.85	4.47	5.60	5.78
MATERA (Matera, Italy)									
Bias	-0.92	0.75	-0.23	-0.30	0.34	0.70	-0.71	0.25	0.62
RMS	7.80	5.69	4.82	3.55	3.65	6.76	3.68	5.32	5.16
NYALES20 (Ny-Ålesund, Spitsbergen, Norway)									
Bias	2.08	0.52	-0.77	-0.98	-0.80	2.08	-0.80	-1.09	1.36
RMS	5.83	3.77	3.55	3.03	3.10	4.34	2.86	3.98	3.81
SESHAN25 (Shanghai, China)									
Bias	2.28	-0.47	-0.70	-1.54	-1.32	3.55	-0.10	-0.71	1.81
RMS	19.03	9.75	7.00	6.89	8.93	16.67	11.36	12.10	11.5
TSUKUB32 (Tsukuba, Japan)									
Bias	-0.93	0.92	-1.21	-0.69	0.33	2.82	-1.13	-0.71	1.39
RMS	6.54	6.15	7.10	4.07	7.49	10.23	3.59	5.33	6.31
WESTFORD (Haystack, USA)									
Bias	-0.09	0.92	0.91	-0.24	0.62	0.60	-0.09	-2.08	0.99
RMS	16.12	7.86	4.81	5.46	7.00	10.40	6.88	8.01	8.32
WETTZELL (Wetzell, Germany)									
Bias	3.50	-1.26	-0.16	-1.72	-1.38	0.40	3.09	0.03	1.99
RMS	25.10	7.91	3.87	6.71	7.94	7.12	15.24	10.19	10.5
mean over all stations									
Bias	1.47	0.73	0.57	0.72	0.64	1.35	0.86	0.75	0.89
RMS	13.15	7.01	5.86	5.05	6.00	9.25	7.14	7.86	7.67

The last column gives the standard deviation of the biases, and the mean RMS over all ACs. The last two rows show the standard deviation of the biases and the mean RMS over the 12 most frequently used sites (Behrend and Baver 2005). The two lower right values are the mean values of the standard deviation of the biases and the mean RMS over the 12 sites and the eight ACs, i.e., the mean values of the last two rows

long time-series of zenith delays due to the correlations between these parameters, which is reflected in the weight factors (Tables 3 and 4).

4.2 VLBI intra-technique comparison

4.2.1 Bias and RMS among the troposphere estimates of IVS ACs

For the assessment of the precision of the ZD combined in this study, the bias and root mean square (RMS), as well as their mean values over the ACs and stations, are

shown in Table 5 for the 12 most frequently used IVS network stations. The values on the right-hand side of Table 5 are the mean values of the standard deviation of the AC biases and the mean RMS for the respective station. The mean standard deviation of the AC biases of ZWD is 0.89 mm (0.72 mm for the ZTD). It is a representative measure for the biases between the solutions of the ACs.

Considering the inhomogeneous analysis options and parameterizations (Sect. 2.2), the intra-technique agreement of VLBI ZD estimates is very good. The mean RMS over the ACs of the ZWD is 7.67 mm (6.40 mm

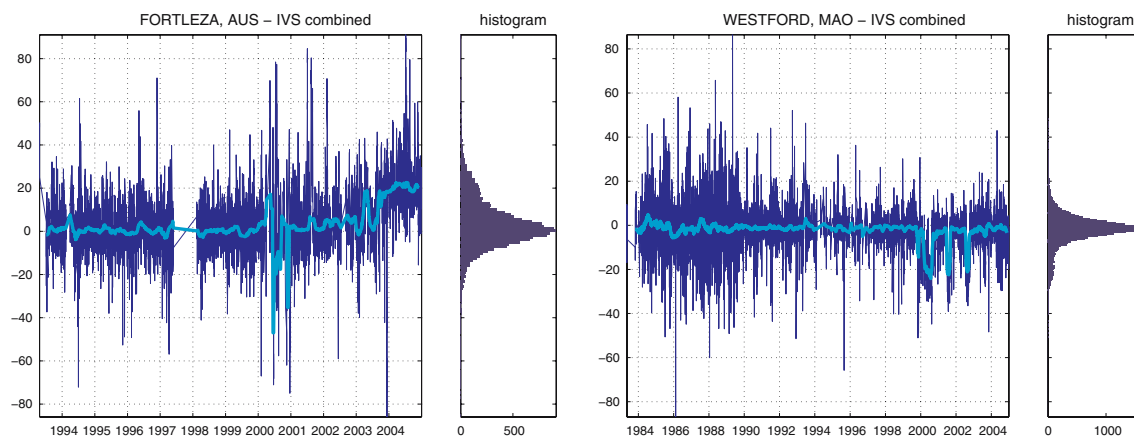


Fig. 3 AUS-IVS combined differential ZWD time-series at station Fortaleza, Brazil, and MAO-IVS combined differential ZWD time-series at station Westford, USA, and 60-day moving medians, as well as histogram plots. Units are mm and the time is given in years. The histogram bins represent integer frequencies

of the corresponding differences. The offset of AUS at Fortaleza in the last year and the outliers at Westford in the MAO solution are probably due to missing in-situ pressure data. The histograms of both stations clearly display disagreement from the Gaussian curve, indicating systematic differences

for the ZTD), and can be interpreted as the precision of the combined IVS long-term series of troposphere parameters. For a comparison of ZWD and ZTD, the contribution of AUS has to be disregarded from the ZWD mean values, because AUS only provides ZWD. The mean values of ZWD without AUS are 0.80 mm for the mean standard deviation of the AC biases and 6.88 mm for the mean RMS.

The mean bias and RMS of ZTD are smaller than those of ZWD. While ZTD can be obtained without additional measurements, the use of in-situ pressure data in the VLBI analysis seems to add further scatter to the ZWD (Tesmer et al. 2007). Other reasons for the disagreements between the ACs could be different procedures of separation of the hydrostatic and wet delays and different treatment of missing in-situ pressure data.

Systematic differences among ACs and among stations can be found; for instance, the application of the RW model (IAA, MAO) and the collocation method (AUS), both seem to produce larger standard deviations in comparison to the PWLF model. Besides the differences of both bias and RMS values between ACs, large differences can be found among the stations: While the mean RMS at Ny-Ålesund, Spitsbergen (3.81 mm), Matera, Italy (5.16 mm) and Kokee Park, Hawaii (5.78 mm) are below the average (7.67 mm), the mean RMS at Hartebeesthoek, South Africa (9.41 mm), Hobart, Australia (10.0 mm) and Shanghai, China (11.5 mm) are significantly larger. The relatively large RMS at Wettzell, Germany (15.24 mm) is due to uncorrected effects (Sect. 4.1).

Figure 3 presents two differential time-series with regard to the IVS combined series: the AUS solution

for Fortaleza (Brasil) shows a shift of the mean value in the last years of the time-series and the MAO solution for Westford (USA) suffers from outliers. The large offsets of AUS at Fortaleza and of MAO at Westford (Table 5) are probably due to a different treatment of missing in-situ pressure data.

4.2.2 Comparison of the time-series coefficients

The coefficients given in Table 6 are determined by the robust BIBER estimator (Sect. 3.2.1) and are statistically significant. The uncertainties of the coefficients (not shown here) are small (between 0.01 mm and 0.3 mm, or mm/year, respectively) and mainly reflect the number of inherent ZDs.

Generally, the offsets and the annual and semi-annual amplitudes of the various IVS ACs agree within a few mm, whereas the scatter of the linear trends is relatively larger. In contrast to the offset and seasonal components, ranging between several mm to several hundred mm, the size of the linear trends (between zero and several mm/year) is relatively small and thus, variations of the inherent noise component and inconsistencies introduced by the use of different models have a stronger effect.

The disagreement of linear trends is mainly due to the short and unequally sampled time-series. Some of the disagreement is caused by the simple mathematical model (Eq. 4), which becomes obvious by the asynchronous sampling of the ZDs between the solutions of the ACs. To remove these deficiencies, the seasonal model can be extended by additional terms of sinusoids for each station, identified from the spectra (Sect. 3.1.1).

Table 6 Coefficients (Eq. 4) of ZWD using original sampling and linear trends applying synchronized sampling (*). The units are mm, and mm/year for the linear trends, respectively

Coefficient	AUS	BKG	CNR	DGF	GSF	IAA	IGG	MAO	IVS
ALGOPARK (Algonquin Park, Canada)									
<i>a</i>	85.5	87.8	86.2	85.9	87.4	87.7	87.4	85.8	87.1
<i>b</i>	0.20	0.00	-0.14	-0.46	0.04	0.18	0.13	0.24	0.07
<i>b</i> (*)	0.85	1.03	0.94	0.97	1.15	1.44	0.98	1.16	1.07
<i>C</i> ₁	47.0	47.7	52.5	46.5	47.9	50.7	48.3	48.5	47.8
<i>C</i> ₂	12.0	12.4	11.6	11.3	12.6	11.8	11.9	13.1	12.5
FORTLEZA (Fortaleza, Brazil)									
<i>a</i>	261.9	257.0	256.8	256.9	257.4	259.4	257.1	257.1	258.0
<i>b</i>	1.31	-0.34	1.12	-0.13	-0.12	-0.13	-0.07	-0.66	0.00
<i>b</i> (*)	3.63	0.87	0.87	1.12	0.99	0.89	1.21	0.41	1.23
<i>C</i> ₁	52.0	52.9	51.6	53.0	52.4	52.3	53.1	52.4	52.5
<i>C</i> ₂	7.4	6.4	3.2	7.2	6.2	6.9	7.6	7.1	6.8
GILCREEK (Fairbanks, Alaska)									
<i>a</i>	61.9	60.1	60.9	59.3	60.0	62.2	60.0	60.3	60.7
<i>b</i>	0.21	0.43	0.72	0.47	0.40	0.29	0.31	0.36	0.33
<i>b</i> (*)	0.61	0.51	0.49	0.51	0.47	0.63	0.65	0.73	0.55
<i>C</i> ₁	40.2	42.3	41.6	42.4	42.8	42.7	40.9	42.0	41.4
<i>C</i> ₂	17.1	18.6	18.4	18.3	19.2	19.5	18.4	18.8	18.8
HARTRAO (Hatebeesthoek, South Africa)									
<i>a</i>	105.3	106.5	111.9	106.6	104.3	104.4	104.6	103.1	105.1
<i>b</i>	1.76	1.96	-2.21	1.70	1.99	1.88	2.13	2.13	1.82
<i>b</i> (*)	-4.81	-5.36	-5.75	-5.48	-5.16	-4.33	-5.46	-5.04	-5.18
<i>C</i> ₁	54.7	56.6	55.2	56.8	55.3	54.8	55.4	55.3	55.1
<i>C</i> ₂	7.6	7.5	11.4	10.9	8.3	9.4	8.8	9.0	8.5
HOBART26 (Hobart, Tasmania)									
<i>a</i>	84.9	87.1	88.2	83.6	84.9	86.9	84.1	86.4	85.8
<i>b</i>	0.34	0.40	-0.18	0.92	0.36	0.00	0.40	0.23	0.32
<i>b</i> (*)	0.34	0.09	-0.07	-0.04	0.66	0.22	0.44	1.07	0.34
<i>C</i> ₁	17.3	20.9	22.8	20.7	20.3	18.8	18.8	20.1	19.7
<i>C</i> ₂	4.8	4.6	0.7	2.3	3.1	4.0	5.3	4.3	3.9
KOKEE (Kokee Park, Kauai, Hawaii)									
<i>a</i>	95.6	93.9	96.7	93.1	93.9	94.3	93.0	93.1	94.0
<i>b</i>	0.44	0.63	0.50	0.79	0.59	0.68	0.52	0.90	0.65
<i>b</i> (*)	0.47	0.73	0.76	0.65	0.70	0.72	0.69	0.70	0.69
<i>C</i> ₁	17.8	17.9	15.8	17.2	18.1	18.1	17.9	17.8	17.6
<i>C</i> ₂	4.9	4.7	5.4	4.5	4.8	4.4	5.2	5.0	4.8
MATERA (Matera, Italy)									
<i>a</i>	98.9	101.4	98.9	99.6	100.4	100.0	99.6	101.2	100.2
<i>b</i>	-0.05	0.27	0.64	0.40	0.23	0.34	0.07	0.14	0.22
<i>b</i> (*)	2.40	2.14	2.19	2.30	2.43	2.28	2.31	2.22	2.32
<i>C</i> ₁	42.9	44.7	41.2	42.2	44.1	42.5	43.1	44.4	43.4
<i>C</i> ₂	3.1	3.6	5.2	3.7	4.7	2.9	3.3	4.0	3.8
NYALES20 (Ny-Ålesund, Spitsbergen, Norway)									
<i>a</i>	46.6	45.6	45.0	43.1	44.0	46.5	43.7	43.1	44.6
<i>b</i>	1.58	1.30	0.86	1.03	0.92	1.28	1.13	1.16	1.12
<i>b</i> (*)	5.62	5.43	5.26	5.23	5.30	5.22	5.22	5.26	5.33
<i>C</i> ₁	25.1	25.9	26.0	24.6	25.0	24.5	23.3	22.8	24.5
<i>C</i> ₂	10.7	11.0	9.8	9.8	10.5	11.1	10.3	10.6	10.6
SESHAN25 (Shanghai, China)									
<i>a</i>	187.0	182.0	180.5	183.5	182.6	149.8	185.4	180.8	182.7
<i>b</i>	-2.04	0.66	-1.99	-0.95	0.26	-1.76	-1.32	0.42	-0.41
<i>b</i> (*)	7.51	7.20	7.05	7.00	7.07	6.91	6.96	7.17	7.14
<i>C</i> ₁	117.8	118.6	124.8	119.9	118.5	67.6	112.0	119.1	115.9
<i>C</i> ₂	41.9	30.0	35.9	35.3	32.4	10.3	31.6	31.2	33.4
TSUKUB32 (Tsukuba, Japan)									
<i>a</i>	142.8	144.8	144.9	141.8	146.8	146.9	144.2	142.3	145.4
<i>b</i>	-1.67	-2.93	-0.80	-1.95	-2.35	-3.02	-3.13	-2.01	-2.39
<i>b</i> (*)	8.62	8.06	8.12	7.98	7.98	7.75	7.92	8.11	8.09
<i>C</i> ₁	116.2	114.8	113.5	113.7	115.2	113.0	116.6	112.3	113.4
<i>C</i> ₂	25.1	23.0	21.0	25.3	22.3	25.6	24.9	24.9	24.3

Table 6 continued

Coefficient	AUS	BKG	CNR	DGF	GSF	IAA	IGG	MAO	IVS
WESTFORD (Haystack, USA)									
<i>a</i>	109.1	109.1	107.4	105.6	108.8	108.1	108.8	105.8	108.5
<i>b</i>	-0.03	-0.01	-0.32	0.04	0.02	-0.05	-0.04	-0.28	-0.06
<i>b</i> (*)	-2.73	-3.06	-3.05	-3.05	-3.13	-3.09	-2.97	-2.63	-3.02
<i>C</i> ₁	55.1	56.7	56.2	54.0	57.2	54.8	55.6	55.7	54.8
<i>C</i> ₂	15.3	16.2	12.3	15.2	17.1	15.5	16.2	15.7	16.1
WETTZELL (Kötzing, Germany)									
<i>a</i>	90.8	85.8	86.9	84.3	85.5	86.6	90.3	87.3	87.0
<i>b</i>	-0.94	0.33	0.19	0.39	0.38	0.13	-0.79	-0.13	-0.01
<i>b</i> (*)	0.14	0.44	0.37	0.42	0.45	0.38	0.17	0.50	0.36
<i>C</i> ₁	39.9	39.7	40.3	39.7	40.6	40.2	37.5	40.0	39.6
<i>C</i> ₂	6.7	7.2	5.8	7.2	7.7	7.5	8.1	7.1	7.4

Hence, the linear trend component is not independent of the seasonal component, the approximation of the seasonal component affects the estimation of the linear trend as well.

Haas et al. (2003) found the linear trends of ZWD from various techniques at Onsala (Sweden) in better agreement, when using results of common epochs only (synchronized sampling). However, the seasonal model in their study included an annual term only.

The coefficients of CNR differ slightly more with regard to the IVS combined solution and among the ACs, because the solution of CNR includes only sessions starting about 1995. For this reason, the amplitudes of the annual signals significantly differ at Algonquin Park by 4.7 mm and at Shanghai by 8.9 mm. For Hartebeesthoek, the offset of CNR differs by about 5 mm relative to all other AC, because it is not affected by the large shift in the in-situ pressure data at Hartebeesthoek on 1993-05-04 (Heinkelmann et al. 2005a) see Table 9.

The larger differences of the coefficients of AUS might be due to the application of the collocation method. The shift of the mean-value in the last years of AUS at Fortaleza results in a different offset and trend (Sect. 4.3.1).

The solution of IAA for station Shanghai, covers only about 52% of the combined sessions. Since accidentally the larger estimates are missing, mainly the offset is affected. The annual and semi-annual amplitudes of IGG for Wettzell differ by 2.1 and 0.7 mm, respectively. This is probably an effect of the missing models for the thermal deformation of the VLBI telescope and atmospheric loading.

4.3 Inter-technique comparison with the IGS combined ZTD series

The comparison with results from other techniques provides a measure of the accuracy of the IVS combined ZD

series. Similar to VLBI, the signals of GNSS techniques are at radio wavelengths, thus providing an excellent basis for a comparison. The IGS provides a combined product of troposphere estimates on a weekly basis, which is comparable with the combination of the IVS pilot project troposphere (Schuh and Boehm 2003).

Results can be accessed from the Geoforschungszentrum Potsdam (GFZ) at Potsdam (Germany). The available data covers nine years of ZTD starting in 1997, when the IGS was founded; however, neither ZWD nor gradients are provided. The internal consistency of this IGS product is reported to be at the level of 4 to 8 mm (Gendt 2004). The ZTD of the IGS are determined every 2 h, thus, for the comparison, estimates at identical epochs are used (synchronized sampling).

4.3.1 Correction due to the height difference

Correction terms for the ZTDs due to height differences between VLBI and GNSS antenna reference points (ARPs) are found using Saastamoinen (1973):

$$ZTD = \frac{0.0022768 \cdot \left(p + \left(\frac{1255}{T} + 0.05 \right) \cdot e \right)}{1 - 0.0026 \cdot \cos(2\phi) - 0.00028 \cdot H} \quad (22)$$

where ZTD (m) denotes the theoretical ZTD referring to the height *H* of the VLBI ARP or the GPS ARP. The difference of the theoretical ZTD (VLBI – GPS) is used to relate the GPS ZTD to the VLBI ARP. While the total pressure *p* (hPa), the absolute temperature *T* (K), and the relative humidity RH (unitless) can be taken from in-situ records for the VLBI ARPs, corresponding values have to be determined for the height of the GPS ARPs. This was done with Berg (1948):

$$\begin{aligned} p_{GPS} &= p_{VLBI} \cdot (1 - 0.0000226 \cdot \Delta H)^{5.225} \\ T_{GPS} &= T_{VLBI} - 0.0065 \cdot \Delta H \\ RH_{GPS} &= RH_{VLBI} \cdot \exp(-0.0006396 \cdot \Delta H) \end{aligned} \quad (23)$$

where the subscripted quantities refer to the height of the corresponding VLBI or GPS ARP. The height difference, ΔH (km), of the ARPs at a site can be determined from the local tie vector, reported by the IERS.

The water vapor pressure e (hPa) was determined with the Magnus-Tetens formula using the saturation vapor pressure e_0 (hPa):

$$e = RH \cdot e_0$$

$$e_0 = \exp\left(2.3026 \cdot \left(\frac{\alpha \cdot t}{\beta + t} + 0.7858\right)\right) \tag{24}$$

where RH denotes the relative humidity (unitless), t denotes the temperature ($^{\circ}\text{C}$), and $\alpha = 17.27$ and $\beta = 237.7$ ($^{\circ}\text{C}$) are constants.

4.3.2 Bias and RMS between IVS and IGS combined ZTD series

After accounting for the height differences (Sect. 4.3.1), the mean bias of the ZTD (IGS – IVS) over the 12 stations becomes 6.6 mm (Table 7) and only at one co-located site (Fortaleza), the bias exceeds 10 mm. The differences between the IGS and IVS combined time-series are all positive, indicating a systematic difference between the two geodetic techniques.

Schmid et al. (2005) showed that the biases between homogeneously processed GPS and VLBI troposphere estimates become smaller when applying absolute phase center corrections for GPS satellite and receiver antennas. Then, significant remaining biases are found only for GNSS antennas covered by radomes: Fairbanks (Alaska), Ny-Ålesund and Onsala (Sweden).

The mean RMS between the IGS and IVS synchronized time-series of 8.6 mm is somewhat larger than the corresponding value of the VLBI intra-technique

Table 7 Bias and RMS of long time-series of ZTD between IGS and IVS at co-located sites

Station		Common epochs		Bias (mm)	RMS (mm)
IVS	IGS	(%)	Total		
ALGOPARK	algo	15.5	5354	9.9	5.7
FORTLEZA	fort	16.7	5264	12.8	15.2
GILCREEK	fair	25.0	8270	4.2	5.0
HARTRAO	hrao	12.5	3746	6.5	9.0
HOBART26	hob2	6.2	1984	7.6	19.6
KOKEE	kokb	24.0	7769	8.1	8.5
MATERA	mate	10.6	3635	4.8	5.9
NYALES20	nyal	17.3	5232	3.3	5.2
SESHAN25	shao	2.7	553	4.0	8.2
TSUKUB32	tskb	6.8	2264	4.4	9.8
WESTFORD	wes2	15.9	5048	9.4	6.1
WETTZELL	wtzt	26.8	9258	4.6	5.2
Mean		15.0		6.6	8.6

combination (6.4 mm), but reflects the overall agreement of the two space-geodetic techniques in terms of zenith delays. Further consistency could be achieved comparing ZD defined at time intervals of equal length.

In Fig. 4, differences between IGS and IVS combined ZTD are presented. One of the largest offsets is found at station Westford (USA), which is covered by a radome. Although the histogram of the differences of ZTD at Wettzell shows a nearly perfect Gaussian curve (Fig. 4, right), the differential time-series between the two techniques reveals different long-term trends.

This effect is probably due to varying analysis options and orbit determinations used for the GPS analysis, because such systematics do not appear when comparing homogeneously re-processed GPS series (Steigenberger et al. 2007). For the determination of long-term trends the IGS ZD series should be homogeneously re-processed including models of absolute phase center corrections. The small mean fraction of synchronous observations (15.0% with respect to IGS) shows how much both techniques can gain from an inter-technique combination.

4.4 Comparison with simulated ZWD from ECMWF

For validation of the IVS combined series of ZWDs, we made comparisons with the ZWD derived from meteorological data provided by the European Centre for Medium-Range Weather Forecasts (ECMWF), Reading (UK).

4.4.1 Simulation of ZWD from ECMWF

The ZWD based on ECMWF data are determined by numerical integration of the wet refractivity N_w (unitless) given by Davis et al. (1985):

$$N_w = \left[k_2 \frac{e}{T} + k_3 \frac{e}{T^2} \right] Z_w^{-1} \tag{25}$$

where k_2 and k_3 denote empirically determined coefficients, Z_w^{-1} is the inverse compressibility factor of wet air, T is the absolute temperature (K), and e is the water vapor pressure (hPa).

The ECMWF Re-Analysis project (ERA-40) covers data from 1957–09 until 2002–08 (Uppala et al. 2005). We used the ERA-40 reanalysis data until the end of 2001 and thereafter the operational analysis product. The two data sets can be concatenated without imposing inconsistencies (Heinkelmann et al. 2005a). With the ERA-40 and the operational analysis product, the meteorological quantities are provided globally at 23 and 21 pressure levels, respectively, between 1 and 1,000 hPa.

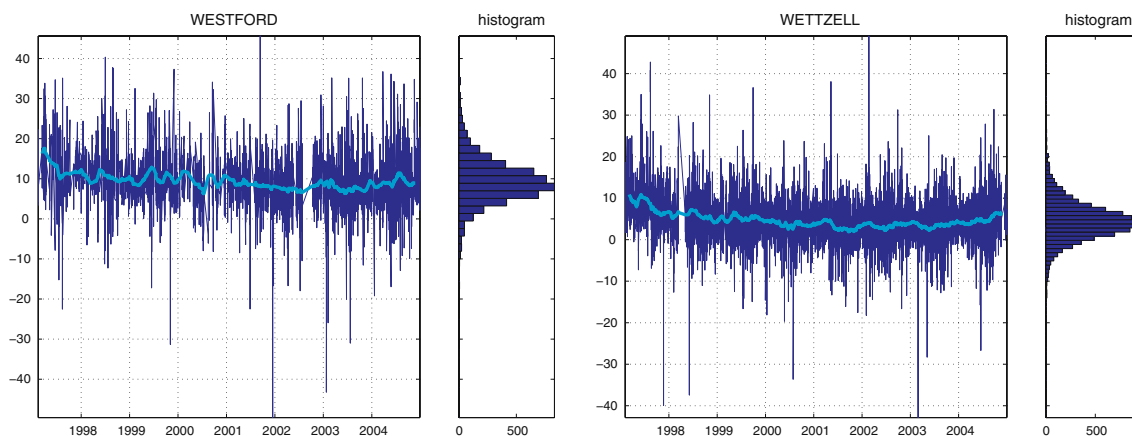


Fig. 4 Differences between IVS and IGS ZTD at Westford, USA, and at Wettzell, Germany, and 60-day moving medians, as well as histogram plots of the differences. Units of the ZTD differences are mm, the time is given in years. The histogram bins represent

integer frequencies of the corresponding differences. Westford shows a significant offset between IGS and IVS combined ZTD series. For Wettzell a slightly different long-term trend can be found and is discussed in the text (Sect. 4.3)

The datasets are given on a grid with a spatial resolution of about 30 km and a temporal resolution of 6 h.

To increase the vertical resolution for the numerical integration, the temperature is interpolated linearly and the total and water vapor pressures are interpolated using exponential approaches (Boehm and Schuh 2003). From the vertical profiles above the stations, ZWD can be determined by integration over the height h from the ARP H up to the height H_0 where the partial pressure of water vapor vanishes (at about 10 km):

$$ZWD = 10^{-6} \sum_{h=H}^{H_0} N_w(h) \delta h \tag{26}$$

where δh (m) denotes the difference between two successive height levels, $N_w(h)$ (unitless) denotes the wet refractivity at the height h .

Considering the different resolution and the interpolations required to derive the information at the station, we expect the simulated ZWD to be smoother than the ones determined by space-geodetic techniques and in-situ pressure records. However, the ZWD from ECMWF data and ZWD from space-geodetic techniques are independent data types and allow a totally independent comparison and validation.

4.4.2 Bias and RMS between IVS combined and ECMWF simulated series

The mean RMS over the 12 stations between ECMWF and IVS combined ZWD series of 20.8 mm is significantly larger than between IGS and IVS ZTD series (8.6 mm). However, the mean bias over the 12 stations of 2.0 mm is relatively small considering the totally

Table 8 Bias and RMS of long time-series of ZWD between ECMWF and IVS

Station	Common epochs		Bias (mm)	RMS (mm)
	(%)	Total		
ALGOPARK	7.5	2419	14.1	22.7
FORTLEZA	18.4	3495	10.5	27.1
GILCREEK	21.5	6904	2.2	11.4
HARTRAO	8.2	2384	5.4	21.4
HOBART26	6.1	1509	1.2	18.4
KOKEE	24.0	4567	0.2	18.9
MATERA	8.2	1909	-13.5	16.7
NYALES20	13.3	2326	-4.0	9.6
SESHAN25	2.2	589	-2.6	27.1
TSUKUB32	6.4	745	-2.1	34.7
WESTFORD	19.1	6145	17.8	21.1
WETTZELL	27.0	8668	-4.8	15.3
Mean	13.5		2.0	20.4

independent approaches and the corresponding value from the IVS–IGS comparison (6.6 mm) (Table 8).

A reason for the biases may be uncorrected offsets in the in-situ pressure data due to height differences between the pressure sensors and the VLBI ARPs. These height differences could not be considered here due to the incompleteness of this information. The status of the data concerning the meteorological sensors at IVS sites is available from the webpage of the 'IVS-MET' Project. While the relatively large biases at Fortaleza and Westford are probably due to missing in-situ pressure data (Fig. 3), the relatively large biases at Algonquin Park and at Matera can not be currently explained.

Again, synchronized sampling is applied for the comparison, and therefore not all the information is used. In fact, the mean percentage of common epochs is only 13.5%. Unlike the ZTD, the ZWD has to be determined using total pressure values. The use of in-situ pressure records adds further measurement errors and thus more scatter to the ZWD estimates. Furthermore, various interpolations are necessary to obtain the ECMWF ZWD at the VLBI site. However, the main reason for the relatively large mean RMS difference could be the fact that the ECMWF quantities are determined from distinct measurements every 6 h, whereas the VLBI ZD represent the integrated water vapor during 1 h of measurement.

Hartebeesthoek, Hobart, Kokee Park and Ny-Ålesund all show significant shifts of the mean value of ZWD. The jumps detected in ZWD series are caused by corresponding jumps in the in-situ pressure records. These artificial breaks can be caused by replacement and relocation of sensors, calibration errors, or uncorrected calibration changes. The homogeneity of the ERA-40 pressure data is very good (Haimberger 2005 and personal communication) during the complete observational history of VLBI (starting in 1979). Therefore, ERA-40 (and operational analysis) pressure data can be used as a reference to identify inconsistencies in the in-situ pressure records used in the analysis of space-geodetic techniques, e.g., shifts of the running mean value, or shifts of the running standard deviation.

The breaks can be found by the standard normal homogeneity test (e.g. Tuomenvirta and Alexandersson 1996), which has been applied to the in-situ pressure records from the IVS network stations earlier (Heinkelmann et al. 2005a). The breaks of ZWD introduced by breaks of the in-situ pressure data have been removed in determining the biases presented in this paper (Table 8). To avoid systematic distortions of the wet and total troposphere estimates, we recommend using homogenized pressure data in the analysis. Inherent breaks of the ZWD introduced by the in-situ pressure data were corrected applying Eq. (3), using the pressure breaks reported in Table 9. The effect of this procedure is shown for Hartebeesthoek in Fig. 5.

5 Conclusions and outlook

We investigated the precision of long-term tropospheric delay estimates from the IVS at 12 representative stations by analysing, comparing and combining solutions from eight IVS ACs including all geodetic VLBI sessions between January 1984 and December 2004. The combined IVS series were validated with corresponding

Table 9 Considered pressure breaks for the determination of bias between IVS and ECMWF ZWD

Station	Epoch	Break (hPa)
ALGOPARK	2003-01-17	-2.8
GILCREEK	1993-06-26	1.4
HARTRAO	1993-05-04	10.0
HOBART26	1991-12-11	17.4
KOKEE	2003-06-17	1.6
NYALES20	1998-07-01	2.8
SESHAN25	1995-04-25	-7.6
WETTZELL	1986-08-07	1.9

estimates from the IGS and with values determined from the ECMWF.

Long time-series from different IVS ACs can be combined at the level of parameter estimates. However, it is necessary to eliminate outliers from the individual time-series. The variance-covariance matrices obtained by different estimation models show significant differences, thus, they have been neglected so far. The weights for the ACs were found by VCE for each station individually. The weights of the ACs differ significantly between the stations, but marginally between ZTD and ZWD.

The combined time-series of zenith delays can be used to perform intra- and inter-technique comparisons and validations. The mean bias of ZWD is 0.89 mm (0.72 mm for ZTD) and the RMS is 7.67 mm (6.40 mm), which shows an overall good agreement between the IVS ACs. Both bias and RMS vary among stations and ACs. The ZWD series have slightly larger mean bias and mean RMS, which can be due to disagreements in the separation of wet and hydrostatic delays and due to the introduction of in-situ pressure measurements, which adds further errors to the estimates.

The estimated coefficients of the time-series model (Eq. 4) generally agree, but in the case of the linear trend component, a better correspondence can be achieved using synchronized sampling. Disagreement among the IVS ACs concerning the separation of ZWD and ZHD and missing in-situ pressure records affects the long-term trends. Future studies should identify possible reasons for the linear trends to differ, and assess the role of the sampling in explaining the deficiencies of the simple time-series model.

The inter-technique comparison of IVS and IGS ZTD combinations shows good overall agreement between the two techniques. A mean bias of 6.6 mm and mean RMS of 8.6 mm are obtained in this study. The biases due to height differences of the ARPs can be removed using local tie vectors. The remaining biases are probably due

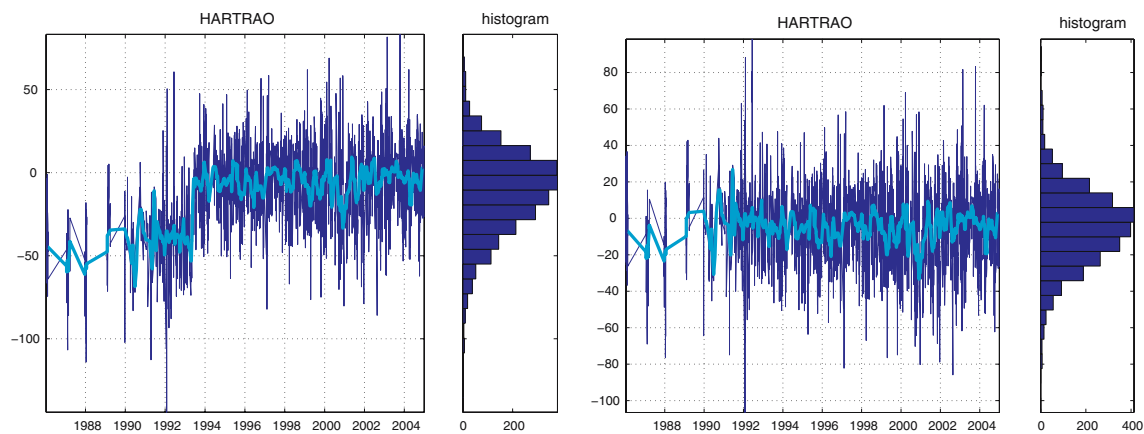


Fig. 5 Differences between IVS and ECMWF ZWD at Hartebeesthoek, South Africa, and 60-day moving medians, as well as histogram plots of the differences. Units of the ZWD differences are mm and the time is given in years. The histogram bins represent integer frequencies of the corresponding differences.

to the unconsidered models of absolute antenna and satellite phase center variations. Different long-term trends were found from the IVS and IGS ZTD time-series for some stations, which can be due to changes in the analysis strategy of the IGS, e.g., new orbit determinations.

Homogeneously reprocessed GPS time-series should significantly improve the long-term stability of the IGS troposphere estimates. It would be advantageous to extend the IGS troposphere products to include ZWD and azimuthal gradients. The general agreement, as well as the different temporal and spatial coverage of VLBI and GNSS ZDs, promise fruitful results for the inter-technique combination of troposphere parameters. The inclusion of troposphere parameters in files of a common format, i.e., the SINEX format, will be among the next steps to achieve this goal.

The mean bias of 2.0 mm and the mean RMS of 20.4 mm between the ZWD time-series of IVS and ECMWF are not as consistent as those between IVS and IGS. In particular, the RMS differences are significantly larger, which is mainly due to the different temporal properties, but also caused by the interpolations of ECMWF. Smaller inconsistencies are introduced by the in-situ pressure measurements used within the VLBI analysis, which suffer from outliers and artificial breaks of the running mean. The breaks have to be identified and removed, e.g. by standard normal homogeneity tests. Future combinations of long-term troposphere series should be done using troposphere parameters obtained with homogenized pressure data.

Because of the high precision of VLBI, its global coverage, and more than 20 years of observational history,

The left figure displays the IVS combined time-series without correction of the break. The shift of the mean value of the ZWD differences is caused by an artificial break of the in situ pressure records at 1993-05-04. For the analysis, homogenized pressure records should be used

we will investigate in future work the potential of VLBI for the validation of meteorological water vapor datasets.

Acknowledgments We greatly acknowledge the IVS and its member institutions. We would like to thank the Zentralanstalt für Meteorologie und Geodynamik (ZAMG), Vienna, Austria, for providing access to the data of the ECMWF and the Austrian Science Fund (FWF), project P16992-N10 “VLBI for climate studies” for supporting this work. The authors would like to thank the reviewers and the editors for their constructive comments.

References

- Altamimi Z, Sillard P, Boucher C (2002) ITRF2000: a new release of the international terrestrial reference frame for Earth science applications. *J Geophys Res* 107(B10):2214. doi:10.1029/2001JB000561
- Behrend D, Cucurull L, Vila J, Haas R (2000) An inter-comparison study to estimate zenith wet delays using VLBI, GPS, and NWP models. *Earth Planets Space* 52:691–694
- Behrend D, Baver K (eds) (2005) International VLBI service for geodesy and astrometry. Annual Report 2004, NASA/TP-2005-212772, NASA, Greenbelt
- Berg H (1948) *Allgemeine Meteorologie*. Dümmler, Bonn, p 337
- Bevis M, Businger S, Chiswell S, Herring TA, Anthes RA, Rocken C, Ware RH (1994) GPS meteorology: mapping zenith wet delays onto precipitable water. *J Appl Met* 33:379–386
- Bierman GJ (1977) Factorization methods for discrete sequential estimation. In: Bellman R (ed), *Mathematics in science and engineering*, vol 128. University of Southern California, p 237
- Boehm J, Schuh H (2003) Vienna Mapping Functions. In: Schwegmann W, Thorandt V (eds), *Proceedings of the 16th working meeting on European VLBI for geodesy and astrometry*, Leipzig, 9–10 May, pp 131–144
- Boehm J, Schuh H (2004) Vienna Mapping Functions in VLBI analyses. *Geophys Res Lett* 31:L01603. doi:10.1029/2003GL018984

- Davis J, Herring TA, Shapiro II, Rogers AEE, Elgered G (1985) Geodesy by radio interferometry: effects of atmospheric modelling errors on the estimates of baseline lengths. *Radio Sci* 20:1593–1607
- Fey AL, Ma C, Arias EF, Charlot P, Feissel-Vernier M, Gontier AM, Jacobs CS, Li J, MacMillan DS (2004) The second extension of the international celestial reference frame: ICRF-Ext.2. *Astron J* 127:3587–3608
- Foerstner W (1979) Ein Verfahren zur Schätzung von Varianz- und Kovarianzkomponenten. *Allg. Vermess. Nachr.* 11–12, pp 446–453
- Gambis D (ed) (1999) First extension of the ICRF, ICRF-Ext.1. 1998 IERS Annual Report, Observatoire de Paris, pp 87–114
- Gendt G (2004) Report of the tropospheric working group for 2002. In: Gowy K, Neilan R, Moore A (eds), 2001–2002 Technical Report IGS Central Bureau, Jet Propulsion Laboratory, Pasadena
- Gradinarsky LP, Haas R, Elgered G, Johansson JM (2000) Wet path delay and delay gradients inferred from microwave radiometer, GPS and VLBI observations. *Earth Planets Space* 52:695–698
- Haas R, Elgered G, Gradinarsky L, Johansson J (2003) Assessing long term trends in the atmospheric water vapor content by combining data from VLBI, GPS, radiosondes and microwave radiometry. In: Schwegmann W, Thorandt V (eds), Proceedings of the 16th working meeting on European VLBI for geodesy and astrometry, Leipzig, 9–10 May, pp 279–288
- Haimberger L (2005) Homogenization of radiosonde temperature time series using ERA-40 analysis feedback information. ERA-40 Project Report Series No. 22, ECMWF, Reading, p 70
- Hampel FR, Ronchetti EM, Rousseeuw PJ, Stahel WA (1986) Robust statistics: the approach based on influence functions. Wiley, New York, p 502
- Heinkelmann R, Boehm J, Schuh H (2005a) Homogenization of surface pressure recordings and its impact on long-term series of VLBI tropospheric parameters. In: Vennebusch M, Nothnagel A (eds), Proceedings of the 17th working meeting on European VLBI for geodesy and astrometry, Noto, 22–23 April, pp 74–78
- Heinkelmann R, Boehm J, Schuh H (2005b) IVS long term series of tropospheric parameters. In: Vennebusch M, Nothnagel A (eds), Proceedings of the 17th working meeting on European VLBI for geodesy and astrometry, Noto, 22–23 April, pp 69–73
- Herring TA (1992) Modelling atmospheric delays in the analysis of space geodetic data. In: Proceedings of refraction of atmospheric signals in geodesy, Netherlands Geodetic Commission Series, vol. 36, The Hague, pp 157–164
- Huber PJ (1981) Robust statistics. Wiley, New York, p 308
- Koch KR (1997) Parameterschätzung und Hypothesentests, 3rd edn. Dümmler, Bonn, p 368
- Krügel M, Thaller D, Tesmer V, Rothacher M, Angermann D, Schmid R (2007) Tropospheric parameters: combination studies based on homogeneous VLBI and GPS data. *J Geod* (this issue)
- Kutterer H, Heinkelmann R, Tesmer V (2003) Robust outlier detection in VLBI data analysis. In: Schwegmann W, Thorandt V (eds), Proceedings of the 16th working meeting on European VLBI for geodesy and astrometry, Leipzig, 9–10 May, pp 247–255
- Lomb NR (1976) Least-squares frequency analysis of unequally spaced data. *Astroph Sp. Sci.* 39:447–462
- Ma C, Arias EF, Eubanks TM, Fey AL, Gontier AM, Jacobs CS, Sovers OJ, Archinal BA, Charlot P (1998) The international celestial reference frame as realized by very long baseline interferometry. *Astron J* 116:516–546
- MacMillan DS (1995) Atmospheric gradients from very long baseline interferometry observations. *Geophys Res Lett* 22(9): 1041–1044
- Niell AE (1996) Global mapping functions for the atmosphere delay at radio wavelength. *J Geophys Res* 101(B2):3227–3246
- Niell AE, Coster AJ, Solheim FS, Mendes VB, Toor PC, Langley RB, Upham CA (2001) Comparison of measurements of atmospheric wet delay by radiosonde, water vapor radiometer, GPS, and VLBI. *J Atmos Ocean Tech* 18:830–850
- Nothnagel A (2000) Der Einfluss des Wasserdampfes auf die modernen raumgestützten Messverfahren. Verlag des Bundesamtes für Kartographie und Geodäsie, Frankfurt (M.), p 75
- Nothnagel A (2003) VTRF2003: A conventional VLBI terrestrial reference frame. In: Schwegmann W, Thorandt V (eds), Proceedings of the 16th working meeting on European VLBI for geodesy and astrometry, Leipzig, 9–10 May, pp 195–199
- Nothnagel A (2005) VTRF2005: a combined VLBI terrestrial reference frame. In: Vennebusch M, Nothnagel A (eds), Proceedings of the 17th working meeting on European VLBI for geodesy and astrometry, Noto, 22–23 April, pp 118–124
- Petrov L, Boy J-P (2004) Study of the atmospheric pressure loading signal in very long baseline interferometry observations. *J Geophys Res* 109:B03405. doi:10.1029/2003JB002500
- Roberts DH, Lehar J, Dreher JW (1987) Time series analysis with CLEAN. I. Derivation of a spectrum. *Astron J* Nr 93(4): 968–989
- Saastamoinen J (1973) Contributions to the theory of atmospheric refraction, Part II. *Bull Géod* 107:13–34
- Schlueter W, Himwich E, Nothnagel A, Vandenberg N, Whitney A (2002) IVS and its important role in the maintenance of the global reference systems. *Adv Space Res* 30(2):145–150
- Schmid R, Rothacher M, Thaller D, Steigenberger P (2005) Absolute phase center corrections of satellite and receiver antennas. *GPS Solut* 9. doi:10.1007/s10291-005-0134-x
- Schuh H, Boehm J (2003) Determination of tropospheric parameters within the IVS Pilot Project. *Österreichische Zeitung für Vermessung & Geoinformation (VGI)* 1/2003, pp 14–20
- Schuh H, Panafidina N, Boehm J, Heinkelmann R (2006) Climatic signals observed by VLBI. *Acta Geod Geoph Hung* 41(2). doi:10.1556/AGeod.41.2006.2.2
- Skurikhina E (2001) On computations of antenna thermal deformation in VLBI data processing. In: Behrend D, Rius A (eds), Proceedings of the 15th working meeting on European VLBI for geodesy and astrometry, Barcelona, 7–8 September, pp 124–130
- Snajdrova K, Boehm J, Willis P, Haas R, Schuh H (2005) Multi-technique comparison of tropospheric zenith delays derived during the CONT02 campaign. *J Geod* 79(10–11). doi:10.1007/s00190-005-0010-z
- Steigenberger P, Tesmer V, Krügel M, Schmid R, Thaller D, Vey S, Rothacher M (2007) Comparisons of homogeneously reprocessed GPS and VLBI long time series of troposphere zenith delays and gradients. *J Geod* (this issue)
- Steinforth C, Nothnagel A (2004) Considering a priori correlations in the IVS combined EOP Series. In: Vandenberg NR, Baver KD (eds), IVS 2004 general meeting proceedings, Ottawa, 9–11 February, pp 413–417
- Tesmer V, Boehm J, Heinkelmann R, Schuh H (2007) Effect of different tropospheric mapping functions on the TRF, CRF, and position time-series estimated from VLBI. *J Geod* (this issue)
- Titov O, Schuh H (2000) Short periods in Earth rotation seen in VLBI data analysed by the least-squares collocation method. IERS Technical Note, 28, Observatoire de Paris, pp 33–41
- Titov O, Yakovleva HG (2000) Seasonal variations in radial components of VLBI stations. *Astron Astrophys Trans* 4:591–603

- Titov O, Tesmer V, Boehm J (2004) OCCAM v.6.0 Software for VLBI Data Analysis. In: Vandenberg NR and Baver KD (eds), IVS 2004 general meeting proceedings, Ottawa, 9–11 February, pp 267–271
- Tuomenvirta H, Alexandersson H (1996) Review on the methodology of the standard normal homogeneity test (SNHT). In: Hungarian Meteorological Service (eds), Proceedings of the 1st seminar for homogenization of surface climatological data, Budapest, 6–12 October, pp 35–45
- Uppala SM, Kallberg PW, Simmons AJ, Andrae U, da Costa Bechtold V, Fiorino M, Gibson JK, Haseler J, Hernandez A, Kelly GA, Li X, Onogi K, Saarinen S, Sokka N, Allan RP, Andersson E, Arpe K, Balmaseda MA, Beljaars ACM, van de Berg L, Bidlot J, Bormann N, Caires S, Chevallier F, Dethof A, Dragosavac M, Fisher M, Fuentes M, Hagemann S, Hólm E, Hoskins BJ, Isaksen L, Janssen PAEM, Jenne R, McNally AP, Mahfouf J-F, Morcrette J-J, Rayner NA, Saunders RW, Simon P, Sterl A, Trenberth KE, Untch A, Vasiljevic D, Viterbo P, Woolen J (2005) The ERA-40 Reanalysis. *Q J R Meteorol Soc* 131. doi:10.1256/qj.04.176
- Wicki F (1992) Robuste M - Schätzer und Zuverlässigkeit. Berichte des Instituts für Geodäsie und Photogrammetrie Rep No. 190, Eidgenössische Technische Hochschule Zürich
- Wicki F (1999) Robuste Schätzverfahren für die Parameterschätzung in geodätischen Netzen. Rep No. 67, Mitteilungen des Instituts für Geodäsie und Photogrammetrie an der Eidgenössischen Technischen Hochschule Zürich
- Wicki F (2001) Robust Estimator for the adjustment of geodetic networks. In: Carosio A, Kutterer H (eds), Proceedings of the first international symposium on robust statistics and fuzzy techniques in geodesy and GIS, IAG-SSG 4.190 Non-probabilistic assessment in geodetic data analysis, pp 53–60